

## Calculating Raman spectra of Graphene oxide through Hartree Fock Method

Rashid Nizam<sup>1</sup>,

<sup>1</sup>Centre of Excellence in Material Science, Department of Applied Physics, Aligarh Muslim University, Aligarh, INDIA

---

### ABSTRACT

The investigation has been done of Raman spectra of mono-graphene oxide (GO); bi-graphene oxide and tri-graphene oxide by Hartree Fock calculations interpret available experimental results. The models of this detailed analysis expose that the graphene oxide (GO) is rough with rough average surface of 0.6 nm and the structure is predominantly amorphous due to distortions from  $sp^3$  C-O bonds. About 40%  $sp^3$  bonding was calculated to be present in these sheets with measured O/C ratio of 1:5. These  $sp^2$  to  $sp^3$  bond modifications due to oxidation are also supported by Hartree Fock calculations. Besides the Raman spectra, the polarized depolarization ratio and the unpolarized depolarization ratio each mono-graphene oxide (GO); bi-graphene oxide and tri-graphene oxide has been calculated which almost satisfying the graphene oxide available literature. It is observed that the Raman spectra are increasing as the number of graphene oxide layer.

**Key words:-** Raman spectra, Hartree Fock, and polarized depolarization

---

### INTRODUCTION

Graphene, a one layer of carbon bonded in a honeycomb lattice structure, which has motivated a innumerable of research as of its exceptional electrical, mechanical, and thermal properties.[1–4] The graphene can be made by a mechanical cleavage method [1] or grown epitaxially from surfaces [5] or by CVD method, [6,7] that has a zero-bandgap without semiconducting properties, hamper its application in nanoelectronics. So, it is of grand requirement to unlock the bandgap in graphene. One ways is to make graphene nanoribbons (GNRs), which have been theoretically calculated to be semiconductor with the width reduced down to sub-10 nm.[8,9] This result in semiconductor characteristics come up from the quantum confinement effect in addition to edge effect from the small width.[8–10] Modern experimental progress has discovered such properties with a great promise for real applications, for example in p-type and n-type graphene field effect transistors.[11–13] The GNRs might rival or even replace CNTs in every semiconducting properties because the great chirality is needed for CNTs to be metals or semiconductors.[14,15] Reliable manufacture of such nanoribbons is also required for various investigations.[16] So, how to build GNRs is solution to their applications. A few techniques for building GNRs have been

informed recently.[11,12,17–20] Among them, equally chemically sonicating expandable graphite [11] and physically with chemically unzipping CNTs [12,18] show great agree. GNRs with a width down to 5 nm have been attained that illustrate outstanding electrical performance [11]. Although, new with simple methods are still investigating to produce GNRs for the potential in biology, electronics, magnetism, and catalysis applications [16].

### MATERIAL AND METHODS

#### Model

The structure of graphene oxide is frequently simplistically imagined to be a graphene sheet bonded to oxygen in the form of carboxyl, hydroxyl or epoxy groups. The graphene oxide sheets are irregular with an average roughness of 0.6 nm and the structure is primarily amorphous because of distortions from the high fraction of  $sp^3$  C-O bonds [21]. These graphene oxide films have been found about 40%  $sp^3$  bonding for O/C ratio of 1:5. In this papers the graphene oxide sheets consisting of mono-, bi-, and trilayers can be readily identified in the AFM image shown in Fig 1[21]. The ratio of mono-, bi-, and trilayers of grapheme oxide is 1.6:2.6:3.6

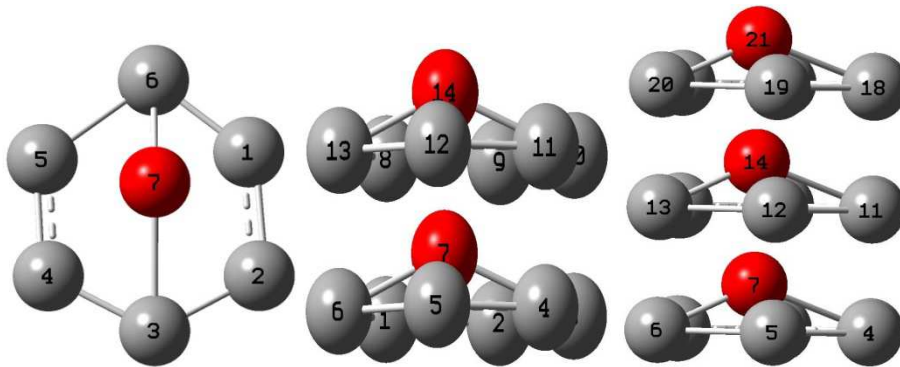


Figure 1 shows mono, bi and tri graphene oxides models layer

#### Calculation

The molecular Hartree-Fock wave function is used to calculate the atomic orbital of molecule (graphene oxide) written as in the product (Slater determinant) form of an antisymmetrized of spin-orbitals, each spin-orbital being a product of a spatial orbital  $\phi_i$  and a spin function (either  $\alpha$  or  $\beta$ ). The term for the Hartree-Fock molecular electronic energy  $E_{HF}$  is specified by the variation theorem

$$E_{HF} = \langle D | \hat{H}_{el} + V_{NN} | D \rangle$$

where D is the Slater determinant Hartree-Fock wave function,  $\hat{H}_{el}$  and  $V_{NN}$  are electrons operator and energy operators of Coulomb interaction of electrons with nuclei respectively.

As  $V_{NN}$  does not include electronic coordinates and D is normalized, thus have  $\langle D | V_{NN} | D \rangle = V_{NN} \langle D | D \rangle = V_{NN}$  The operator  $\hat{H}_{el}$  is the sum of two- electron operators  $\hat{g}_{ij}$  and one-

electron operators  $\hat{f}_i$ ; so  $\hat{H}_{el} = \sum_i \hat{f}_i + \sum_j \sum_{i>j} \hat{g}_{ij}$ , where  $\hat{f}_i = -\frac{1}{2} \nabla_i^2 - \sum_{\alpha} Z_{\alpha} / r_{i\alpha}$  and  $\hat{g}_{ij} = 1 / r_{ij}$

The Hamiltonian  $\hat{H}_{el}$  remain same as the Hamiltonian H for an atom except that  $\sum_{\alpha} Z_{\alpha} / r_{i\alpha}$  replaces  $Z_{\alpha}$  in  $\hat{f}$ . Hence, the Hartree-Fock energy of a diatomic or polyatomic molecule with only closed shells is

$$E_{HF} = 2 \sum_{i=1}^{n/2} H_{ii}^{core} + \sum_{i=1}^{n/2} \sum_{j=1}^{n/2} (2J_{ij} - K_{ij}) + V_{NN} \quad (1)$$

$$\begin{aligned} H_{ii}^{core} &\equiv \langle \phi_i(1) | \hat{H}^{core}(1) | \phi_i(1) \rangle \\ &\equiv \langle \phi_i(1) | -\frac{1}{2} \nabla_1^2 - \sum_{\alpha} \frac{Z_{\alpha}}{r_{1\alpha}} | \phi_i(1) \rangle \\ J_{ij} &\equiv \langle \phi_i(1) \phi_j(2) | 1/r_{12} | \phi_i(1) \phi_j(2) \rangle \\ K_{ij} &\equiv \langle \phi_i(1) \phi_j(2) | 1/r_{12} | \phi_j(1) \phi_i(2) \rangle \end{aligned}$$

where the one-electron-operator symbol was altered from  $\hat{f}$  to  $\hat{H}^{core}(1)$ . The one- electron core Hamiltonian

$$\hat{H}^{core}(1) \equiv -\frac{1}{2} \nabla_1^2 - \sum_{\alpha} \frac{Z_{\alpha}}{r_{1\alpha}}$$

is the addition of the kinetic-energy operator for electron 1 and the potential-energy operators for the attractions between electron 1 and the nuclei;  $\hat{H}^{core}(1)$  excludes the interactions of electron 1 with the other electrons. The additions over i and j are over the  $n/2$  occupied spatial orbitals  $\phi_i$  of the i -electron molecule. In the Coulomb integrals  $J_{ij}$  as well as the exchange integrals  $K_{ij}$ , the integration goes over the spatial coordinates of electrons 1 and 2.

The Hartree-Fock method come across for those orbitals  $\phi_i$  that minimize the variational integral  $E_{HF}$ . Obviously, each MO is taken to be normalized:  $\langle \phi_i(1) | \phi_i(1) \rangle = 1$ . Moreover, for computational convenience one takes the MOs to be orthogonal:  $\langle \phi_i(1) | \phi_j(1) \rangle = 0$  for  $i \neq j$ . The closed- shell orthogonal Hartree-Fock MOs satisfy

$$\hat{F}(1)\phi_i(1) = \varepsilon_i \phi_i(1) \quad (2a)$$

where  $\varepsilon_i$  is the orbital energy and where the (Hartree-) Fock operator  $\hat{F}$  is (in atomic units)

$$\hat{F}(1) = \hat{H}^{core}(1) + \sum_{j=1}^{n/2} [2\hat{J}_j(1) - \hat{K}_j(1)] \quad (2b)$$

$$\hat{H}^{core}(1) \equiv -\frac{1}{2} \nabla_1^2 - \sum_{\alpha} \frac{Z_{\alpha}}{r_{1\alpha}}$$

where the Coulomb operator  $\hat{J}_j$  and the exchange operator  $\hat{K}_j$ , are defined by

$$\hat{J}_j f(1) = f(1) \int |\phi_j(2)|^2 \frac{1}{r_{12}} dv_2$$

Here  $f$  is an arbitrary function that wills integral over definite integrals all space. The first term on the right is the operator for the kinetic energy of one electron while the second term is the potential-energy operators for the attractions between one electron and the nuclei. The Coulomb operator

$\hat{J}_j(1)$  is the potential energy of interaction between electron 1 and a spread-out electron with electronic density  $-\phi_i(2)^2$ ; the factor 2 in come about due to there is two electrons in each spatial orbital. The exchange operator has no simple physical interpretation but begins from the requirement that the wave function be antisymmetric with respect to electron exchange. From the Hartree equations, the exchange operators are not present. In  $\phi_i$  the Hartree-Fock MOs are eigenfunctions of the same operator  $\hat{F}$ , with the eigenvalues being the orbital energies  $\epsilon_i$ . The orthogonality of the MOs greatly simplifies MO calculations, causing many integrals to vanish. The true Hamiltonian operator and wave function involve the coordinates of all n electrons. The Hartree-Fock Hamiltonian operator  $\hat{F}$  is a one-electron operator (that is, it involves the coordinates of only one electron), and is a one-electron differential equation. This has been indicated in by writing  $\hat{F}$  and  $\phi_i$  as functions of the coordinates of electron 1; of course, the coordinates of any electron could have been used. The operator  $\hat{F}$  is peculiar in that it depends on its own eigenfunctions, which are not known initially. Hence the Hartree-Fock equations must be solved by an iterative process.

To obtain the expression for the orbital energies  $\epsilon_i$  we multiply (2) by  $\phi_i^*(1)$  and integrate over all space. Using the fact that  $\phi_i$  is normalized and equation (1), we obtain

$$\begin{aligned} \epsilon_i &= \int \phi_i^*(1) \hat{F}(1) \phi_i(1) dv_1 \\ \epsilon_i &= \langle \phi_i(1) | \hat{H}^{core}(1) | \phi_i(1) \rangle + \sum_j [2 \langle \phi_i(1) | \hat{J}_j(1) | \phi_i(1) \rangle - \langle \phi_i(1) | \hat{K}_j(1) | \phi_i(1) \rangle] \\ \epsilon_i &= H_{ii}^{core} + \sum_{j=1}^{n/2} (2J_{ij} - K_{ij}) \end{aligned} \quad (3)$$

where  $H_{ii}^{core}$ ,  $J_{ij}$  and  $K_{ij}$  are above defined in the equations.

summing up equation (3) over the n/2 occupied orbitals gives

$$\sum_{i=1}^{n/2} \epsilon_i = \sum_{i=1}^{n/2} \hat{H}_{ii}^{core} + \sum_{i=1}^{n/2} \sum_{j=1}^{n/2} (2J_{ij} - K_{ij})$$

Work out this equation for  $\sum_i H_{ii}^{core}$  and replacing the result into (1), we obtain the Hartree-Fock energy as

$$E_{HF} = 2 \sum_{i=1}^{n/2} \epsilon_i - \sum_{i=1}^{n/2} \sum_{j=1}^{n/2} (2J_{ij} - K_{ij}) + V_{NN}$$

Since there are two electrons per MO, the quantity  $2 \sum_i \epsilon_i$  is the sum of the orbital energies. Subtraction of the double sum in (1) avoids counting each inter electronic repulsion twice. A feasible calculation of accurate molecular SCF wave functions was Roothaan's 1951 proposal to expand the spatial orbitals  $\phi_i$  as linear combinations of a set of one-electron basis functions  $x_s$

$$\phi_i = \sum_{s=1}^b c_{si} x_s \tag{4}$$

To precisely represent the MOs  $\phi_i$ , the basis functions should figure a complete set. This necessitates an infinite number of basis functions. But in practice, one must use a finite number  $b$  of basis functions. If  $b$  is large enough with the functions  $x_s$  well chosen, one can represent the MOs with negligible error. To avoid confusion, we shall use the letters  $r, s, t, u$  to label the basis functions  $x$ , and the letters  $i, j, k, l$  to label the MOs  $\phi$ . Substitution of the expansion (4) into the Hartree-Fock equations (2) gives

$$\sum_s c_{si} \hat{F} x_s = \epsilon_i \sum_s c_{si} x_s \tag{5}$$

Multiplication by  $x_r^*$  and integration gives

$$\sum_{s=1}^b c_{si} (F_{rs} - \epsilon_i S_{rs}) = 0, r = 1, 2, \dots, b \tag{6}$$

$$F_{rs} \equiv \langle x_r | \hat{F} | x_s \rangle, S_{rs} \equiv \langle x_r | x_s \rangle \tag{7}$$

The equations (6) form a set of  $b$  simultaneous linear homogeneous equations in the  $b$  unknowns  $c_{si}$   $s = 1, 2, \dots, b$ , that explain the MO  $\phi_i$  in (5). For a nontrivial solution, one must have

$$\det(F_{rs} - \epsilon_i S_{rs}) = 0 \tag{9}$$

This is a secular equation whose roots provide the orbital energies  $\epsilon_i$ . After getting the occupied-MO expressions as linear combinations of the basis functions, as in (4) equation. This initial set of MOs is used to compute the Fock operator  $F$  from (2b) to (6). The matrix elements (7) are computed, and the secular equation (9) is solved to give an initial set of  $\epsilon_i$ 's. These  $\epsilon_i$ 's used to solve (6) for an improved set of coefficients, giving an improved set of MOs, which are then used to compute an improved  $F$ , and so on. These matrix elements then convert into Raman invariants tensor.

When single crystals of a material are not available then the symmetries of Raman excitations can be studied by measuring the polarization of the scattered light in unoriented samples. Hence one can resolve Raman tensor invariant [29] [30] which yield information about the symmetry, although the assignment is not always unique.

Let us assume a phonon with a diagonal Raman tensor with three elements  $a_1 \neq a_2 \neq a_3$ . Furthermore, the scattering configuration in the laboratory frame is (ZZ). To find the Raman intensity one integrate as well as average over all possible orientations of the crystal. By Euler's angles [31] [32].

$$I_{ZZ} = \frac{1}{8\pi^2} \int_0^{\pi, 2\pi, 2\pi} |e_i \cdot R \cdot e_s|^2 d\Psi d\varphi \sin \nu d\nu$$

$$I_{zz} = \frac{1}{8\pi^2} \int_0^{\pi, 2\pi, 2\pi} \left\langle \begin{pmatrix} \sin \varphi \sin \nu \\ \cos \varphi \sin \nu \\ \cos \nu \end{pmatrix} \begin{pmatrix} a_1 \\ a_2 \\ a_3 \end{pmatrix} \begin{pmatrix} \sin \varphi \sin \nu \\ \cos \varphi \sin \nu \\ \cos \nu \end{pmatrix} \right\rangle^2 d\Psi d\varphi \sin \nu d\nu$$

integrating and rearranging yields

$$I_{zz} = \frac{45\bar{\alpha}^2 + 4\gamma_s'^2}{45} \tag{10}$$

$$\bar{\alpha} = \frac{1}{3}(a_1 + a_2 + a_3) \text{ with}$$

$$\gamma_s'^2 = \frac{1}{2} \left[ (a_1 - a_2)^2 + (a_2 - a_3)^2 + (a_3 - a_1)^2 \right]$$

The result in Eq. (10) embraces for all parallel polarizations of the incoming with outgoing linearly polarized light and for every Raman tensor excluding that  $\gamma_s'^2$ . For perpendicular linear

polarization, e.g.,  $I_{xz}$  the integration yields  $I_{xz} = \frac{3\gamma_s'^2}{45}$ . Now it turn out to be noticeable that the symmetry can also be partially presumed from experiments on unoriented materials.

The intensity on unoriented substances pursues directly from the transformation of a tensor under rotation. A second-rank tensor can be decomposed with respect to the rotation group into a scalar (tensor of rank zero), an antisymmetric matrix (rank one), and a symmetric traceless matrix (rank two). These irreducible components have well defined quantum numbers and transformation properties under rotation. The matrix element for a fixed orientation is obtained from the Wigner-Eckart theorem and the integration over all crystal orientations is determined by the tensor invariants. Different authors use slightly different invariants in Raman scattering. By Neslor and spiror [33] one can define the isotropic invariant

$$\bar{\alpha} = \frac{1}{3}(\alpha_{xx} + \alpha_{yy} + \alpha_{zz})$$

the antisymmetric anisotropy

$$\gamma_{as}^2 = \frac{3}{4} \left[ (\alpha_{xy} - \alpha_{yx})^2 + (\alpha_{xz} - \alpha_{zx})^2 + (\alpha_{yz} - \alpha_{zy})^2 \right]$$

and the symmetric anisotropy

$$\gamma_s^2 = \frac{1}{2} \left[ (\alpha_{xx} - \alpha_{yy})^2 + (\alpha_{yy} - \alpha_{zz})^2 + (\alpha_{zz} - \alpha_{xx})^2 \right] + \frac{3}{4} \left[ (\alpha_{xy} + \alpha_{yx})^2 + (\alpha_{xz} + \alpha_{zx})^2 + (\alpha_{yz} + \alpha_{zy})^2 \right]$$

where  $\alpha_{ij}$  ( $i, j = x, y, z$ ) are the elements of the Raman matrix as given in Table 1 for carbon nanotubes.

$A_{1(g)}$	$A_{2(g)}$	$E_{1(g)}$	$E_{1(g)}$	$E_{2(g)}$	$E_{2(g)}$
$\begin{pmatrix} a & 0 & 0 \\ 0 & a & 0 \\ 0 & 0 & b \end{pmatrix}$	$\begin{pmatrix} 0 & e & 0 \\ -e & 0 & 0 \\ 0 & 0 & 0 \end{pmatrix}$	$\begin{pmatrix} 0 & 0 & c \\ 0 & 0 & 0 \\ d & 0 & 0 \end{pmatrix}$	$\begin{pmatrix} 0 & 0 & 0 \\ 0 & 0 & -c \\ 0 & -d & 0 \end{pmatrix}$	$\begin{pmatrix} 0 & f & 0 \\ f & 0 & 0 \\ 0 & 0 & 0 \end{pmatrix}$	$\begin{pmatrix} -f & 0 & 0 \\ 0 & f & 0 \\ 0 & 0 & 0 \end{pmatrix}$

A linear combination of the tensor invariants can be expressed in the scattering intensity on an unoriented sample in any scattering configuration. For linear parallel ( $\parallel$ ) and perpendicular ( $\perp$ ) polarization of the incoming and scattered light the intensities are given by (apart from a constant factor

$$I_{||} = 45\bar{\alpha}^2 + 4\gamma_s^2 \quad I_{\perp} = 3\gamma_s^2 + 5\gamma_{as}^2$$

which is the generalized result of Equation(10). The quotient  $I_{\perp}/I_{||}$  is known as the depolarization ratio  $\rho$ . Under Placzek's polarizability approximation, it is known that the depolarization ratio of a totally symmetric vibrational mode is less than 0.75, and that of the other modes equals 0.75. A Raman band whose depolarization ratio is less than 0.75 is called a P- depolarization band, and a band with a 0.75 depolarization ratio is called a U-depolarization band. The Raman intensities for any polarization on arbitrarily oriented systems can be implicit through the matrix element for a particular Raman tensor and taking the averaged over Euler's angles. For generality, the result of graphene oxide Raman tensor of into any two rank tensor. This transformation of tensor are can be prescribed by irreducible spherical tensors, that is a break up

into the rotation group. The irreducible spherical tensors  $T_m^{(j)}$  have quick j and m quantum numbers under turning round that can be simply transform according to

$$T_m^{(j)} = \sum_p T_p^{(j)} D_{pm}^{(j)}(\psi, \theta, \phi)$$

where  $D^{(j)}$  is the matrix expression of the rotation group (rotation matrices). The rank k tensor can reduce into irreducible tensor of ranks 0, 1, 2, 3...k with help of the Clebsch-Gordan coefficients. A normalized Raman tensor  $R = T^{(0)} + T^{(1)} + T^{(2)}$  set are converted into irreducible tensors is given by

$$T_0^{(0)} = -\frac{1}{3}(\alpha_{xx} + \alpha_{yy} + \alpha_{zz})$$

$$T_0^{(1)} = \frac{1}{\sqrt{2}}(\alpha_{xy} - \alpha_{yx})$$

$$T_{\pm 1}^{(1)} = \frac{1}{2}[(\alpha_{zx} - \alpha_{xz}) \pm (\alpha_{zy} - \alpha_{yz})]$$

$$T_{\pm 1}^{(2)} = \mp \frac{1}{2}[(\alpha_{zx} + \alpha_{xz}) \pm (\alpha_{zy} + \alpha_{yz})]$$

$$T_{+2}^{(2)} = \frac{1}{2}[(\alpha_{xx} - \alpha_{yy}) \pm i(\alpha_{xy} + \alpha_{yx})]$$

$$T_0^{(2)} = \frac{1}{\sqrt{6}}(2\alpha_{zz} - \alpha_{xx} - \alpha_{yy})$$

In a fixed scattering configuration, the intensity matrix element  $I_{LS}$  is computed through the Wigner-Eekart theorem. An average of irreducible spherical tensors over the randomly oriented graphene oxide molecules is specified by.

$$I_{LS} \propto |e_l \text{Re}_s|^2 = \int_{\Omega} \left| \sum_J e_l T^{(J)} e_s \right|^2 d\omega$$

$$I_{LS} = \int_{\Omega} \left\{ \sum_{J,M} \langle J_i m_i | T_M^{(J)} | J_s m_s \rangle \right\}^2 d\omega$$

where  $(J_i J_s - m_i m_s | J - M)$  are the Clebsch-Gordan coefficients with the selection rule  $\mathbf{M} = m_i - m$ . This gives

$$I_{LS} = \int_{\Omega} \left\{ (J_i J_S - m_i m_S |J[m_S - m_i]) \left\langle \sum_p T_p^{(J)} D_{p(m_S - m_i)}^{(J)} \right\rangle \right\}^2 d\omega$$

The rotation matrices are orthonormal

$$\int_{\Omega} D_{k_1 \mu_1}^{(j_1)*} D_{k_2 \mu_2}^{(j_2)} d\omega = \frac{\Omega}{\sqrt{2j_1 + 1}} \delta_{j_1 j_2} \delta_{k_1 k_2} \delta_{\mu_1 \mu_2} \quad (11)$$

So, each of the contribution of different irreducible tensors rank J can solve break up. Thus the orthonormality of the turning round matrices diminishes to

$$I_{LS}^J \propto (J_i J_S - m_i m_S |J[m_S - m_i])^2 \frac{1}{2J + 1} \sum_p [T_p^{(J)}]^2$$

The sum over p is self-determining of the angular momentum quantum numbers m which formulate to be calculated only once for every J under consideration. As the mixed elements in the squared sum do not necessarily cancel so care should be taken while adding over p by using orthogonality of the rotation matrices in Eq.

For  $I_{LS}^J$  calculation  $\sum_p [T_p^{(J)}]^2$  has to sum  $J = 0, 1, 2$  with the irreducible tensors in Equation (11).

## RESULT AND DISCUSSION

Raman spectroscopy is a widely used tool for the characterization of carbon products, especially considering the fact that conjugated and double carbon-carbon bonds lead to high Raman intensities. However, we are aware of only one previous computational study that investigated the Raman spectra of oxidized nanotubes modeled by relatively short nanotube segments. This geometry introduced imitation features into the vibrational modes, making the interpretation of the experimental spectroscopic features somewhat challenging. Since most GO models involve a mostly intact hexagonal carbon lattice, placing chemical groups randomly throughout the 2D sheet and not on the edges should model the GO structure more accurately.

The rotational constants in x, y, and z axis in the monolayer graphene oxide are 6.6510239, 6.0103342 and 3.3347958 (GHz) respectively. Similarly the rotational constants in x, y, and z axis in the bi-layer graphene oxide are rotational constants are 1.9728517, 1.8545352 and 1.6665593(GHz) respectively. Similarly the rotational constants in x, y, and z axis in the tri-layer graphene oxide are rotational constants are 1.11214180, 0.7828646 and 0.7547065 respectively. The monolayer graphene oxide, bi-layer graphene oxide, and tri-layer graphene oxide has 35 basis function, 105 primitive gaussians, 35 cartesian basis functions, 22 alpha electrons, 22 beta electrons; 70 basis functions, 210 primitive gaussians, 70 cartesian basis functions, 44 alpha electrons, 44 beta electrons; and 105 basis functions, 315 primitive gaussians, 105 cartesian basis function, 66 alpha electrons 66 beta electrons respectively. The nuclear repulsion energy of monolayer graphene oxide, bi-layer graphene oxide and tri-layer graphene oxide is 949.4127854629 Hartrees 242.7200087572 Hartrees and 1947.2886258435 Hartrees respectively. The monolayer graphene oxide, bi-layer graphene oxide, and tri-layer graphene oxide has done SCF E(RHF) = -297.168946620 A.U. after 26 cycles E(RHF) = -593.725114254 A.U. after 35 cycles and E(RHF) = -890.189598584 A.U. after 47 cycles with convergence = 0.5409D-08, 0.3359D-08 and 0.3608D-08 respectively.

Structured graphite has only a couple of Raman-active bands visible in the spectra (Figure 1), the in-phase vibration of the graphite lattice (G band) at  $1638.9\text{ cm}^{-1}$  as well as the (weak) disorder band caused by the graphite edges (D band) at approximately  $517.369, 1033.55$  and  $1354.75\text{ cm}^{-1}$ . These monolayer graphene oxide simulated peaks  $517.369, 1033.55$  and  $1354.75\text{ cm}^{-1}$  are almost observed in graphene oxide experimental work with one simulated peak  $1638.9\text{ cm}^{-1}$  is observed in different papers. [34, 35, 36] The bi-layer graphene oxide simulation peaks obtained are  $416.397, 556.849, 1045.94, 1403.79, 1691.43,$  and  $1971.52\text{ cm}^{-1}$ . The tri layer graphene oxide simulation peaks obtained are  $415.267, 487.608, 563.46, 855.59, 1004.65, 1372.82, 1420.79, 1582.41, 1639.02, 1773.94,$  and  $1997.69\text{ cm}^{-1}$ .

The polarized depolarization ratio and the unpolarized depolarization ratio of the simulated monolayer graphene oxide with respect of raman spectra are  $0.6012, 0.1519, 0.3484, 0.1724$  and  $0.751, 0.2637, 0.5167, 0.2941$  respectively. Similarly the polarized depolarization ratio and the unpolarized depolarization ratio of the simulated bi-layer graphene oxide with respect of raman spectra are  $0.5547, 0.2851, 0.4028, 0.7379, 0.6077, 0.3743$  and  $0.7135, 0.4437, 0.5742, 0.8492, 0.756, 0.5447$  respectively. Similarly the polarized depolarization ratio and the unpolarized depolarization ratio of the simulated tri-layer graphene oxide with respect of raman spectra are  $0.3435, 0.1673, 0.3172, 0.5482, 0.6949, 0.7157, 0.234, 0.2774, 0.3286, 0.2425, 0.3752$  and  $0.5114, 0.2866, 0.4816, 0.7082, 0.82, 0.8343, 0.3792, 0.4344, 0.4946, 0.3904, 0.5457$  respectively. It is observed after simulation that as the number of graphene oxide layers increase, the raman spectra also increase due to increase in modes of graphene oxide vibration.

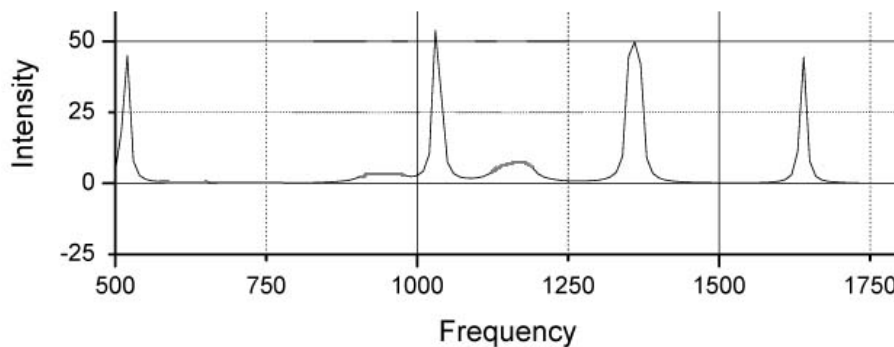


Figure 2 shows Raman spectrum of mono graphene oxide layer

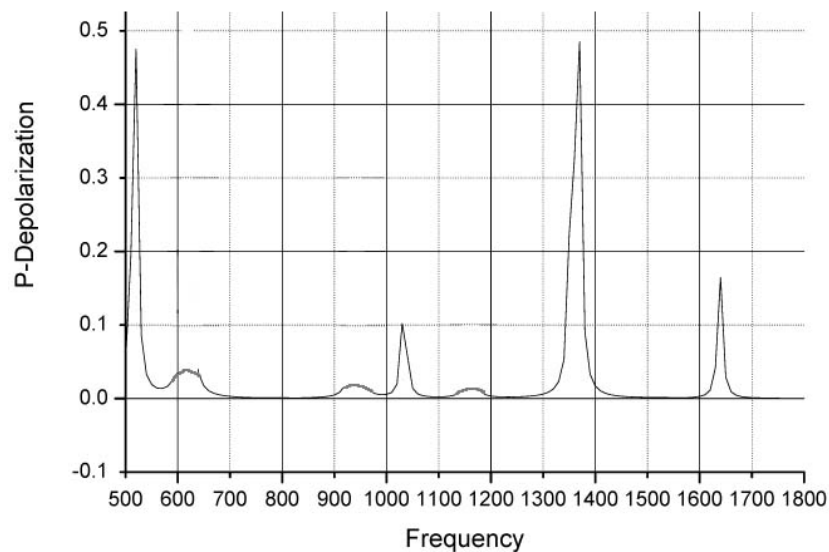
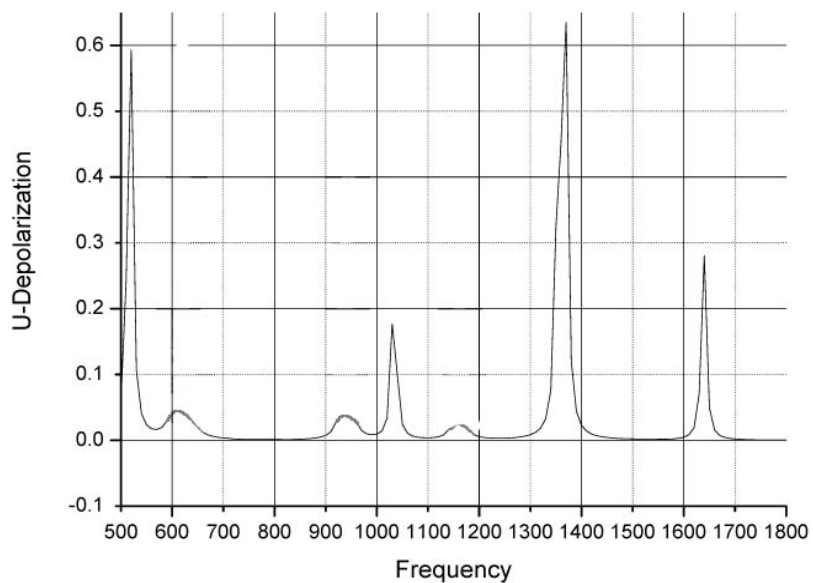
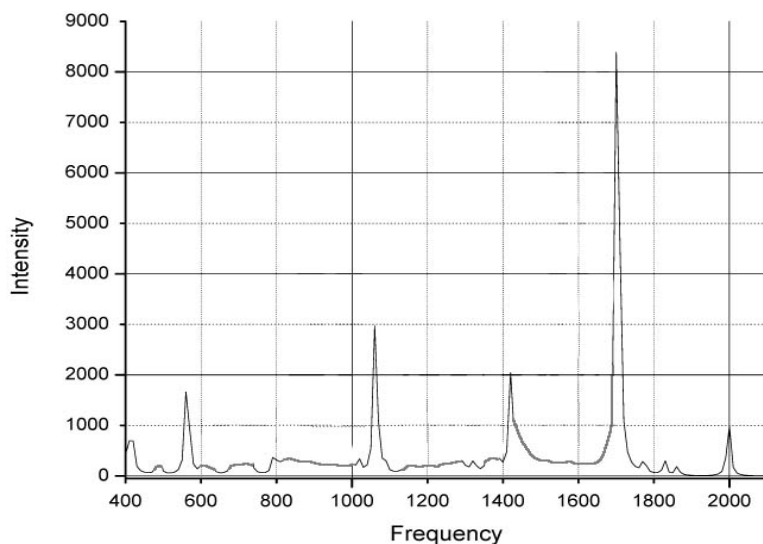


Figure 3 shows P-polarization spectrum of mono graphene oxide layer



**Figure 4 shows U-polarization spectrum of mono graphene oxide layer**



**Figure 5 shows Raman spectrum of bi graphene oxide layer**

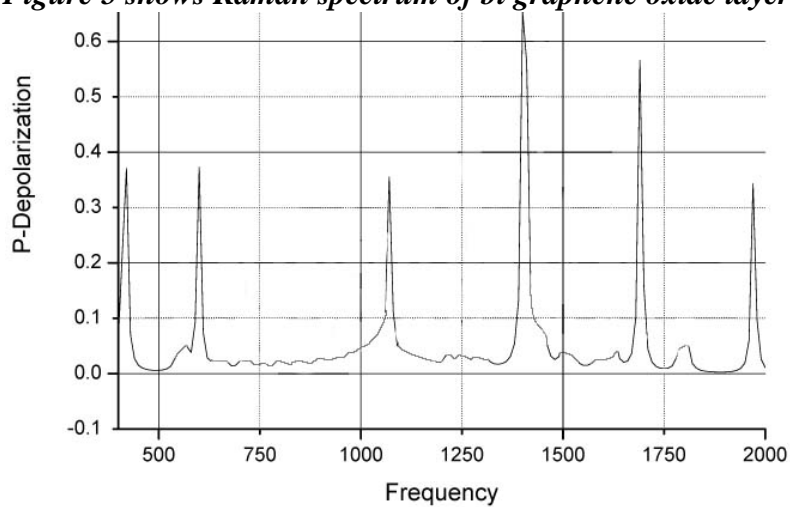


**Figure 6 shows P-polarization spectrum of bi graphene oxide layer**

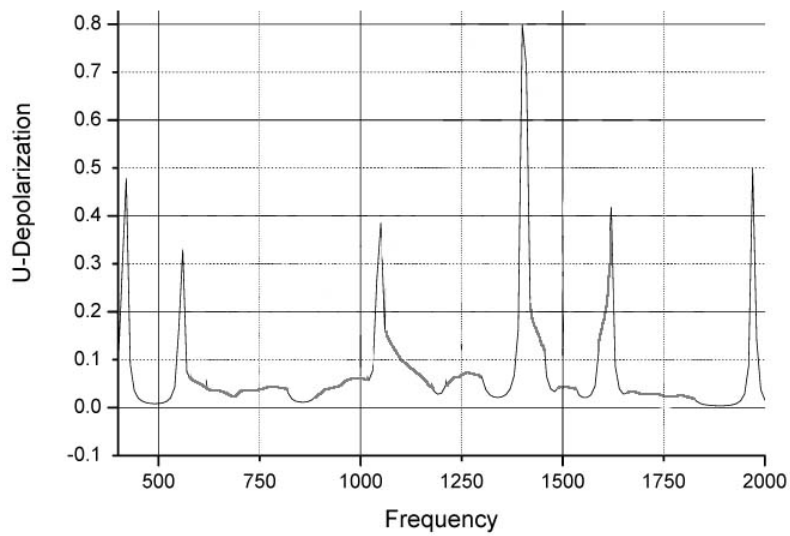


*Figure 7 shows U-polarization spectrum of bi graphene oxide layer*

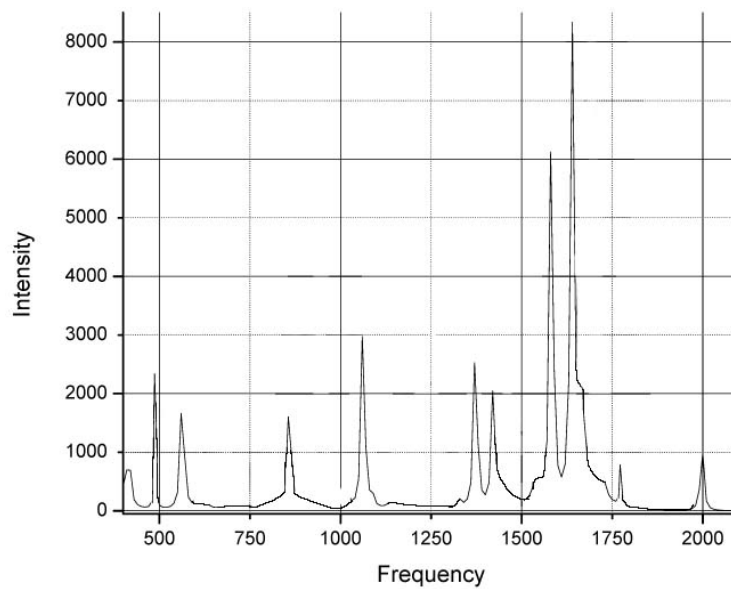


*Figure 8 shows Raman spectrum of tri graphene oxide layer*

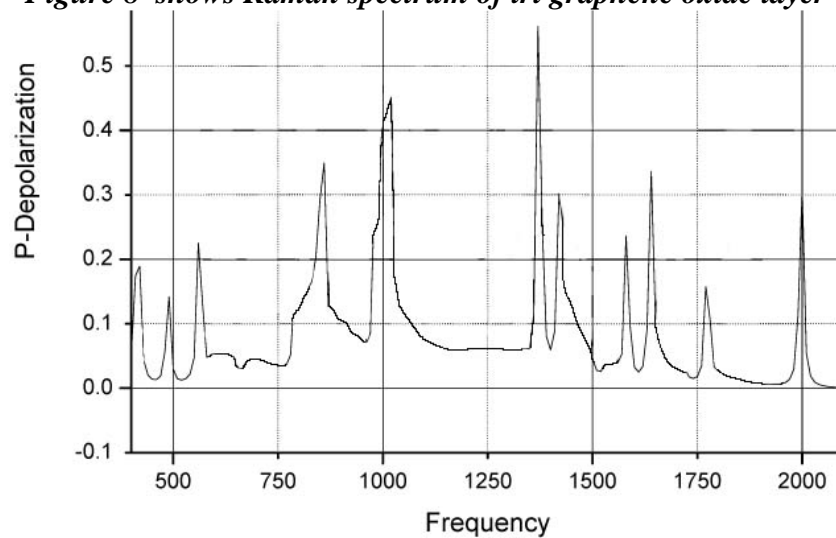


*Figure 9 shows P-polarization spectrum of tri graphene oxide layer*

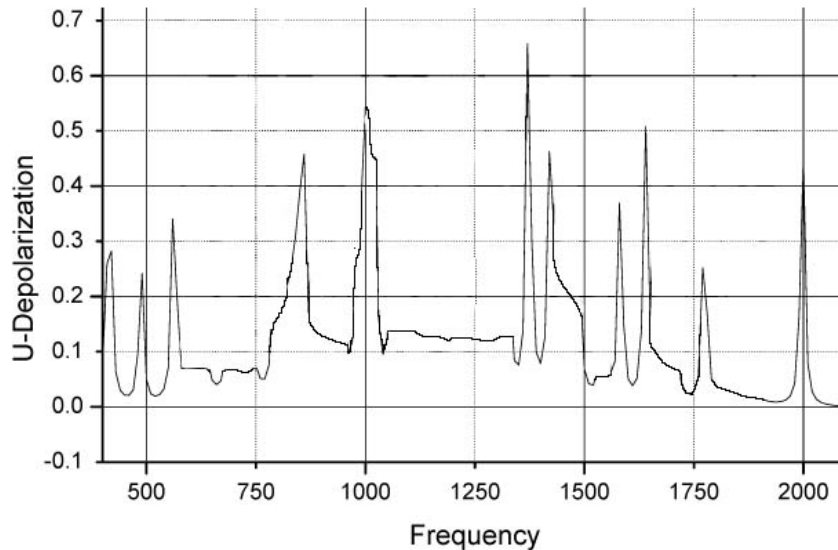


*Figure 10 shows P-polarization spectrum of tri graphene oxide layer*

## CONCLUSION

All spectral features are become visible in the Raman spectra of graphene oxide that provide important characterization information about graphene oxide, with complementary information supplied by ensembles of graphene oxide in graphene oxide bundle. Stress is given both to Raman spectroscopy for 1D systems and to the use of Raman spectroscopy to characterize the graphene oxide structure, defects, and the various environmental effects encountered by graphene oxide. Raman spectroscopy is also closely attached to PL spectroscopy of semiconducting SWNTs, since both experimental techniques are strongly sensitive to the transition energies of individual SWNTs and graphene oxide, to their electronic density of states, and to their interactions. Grouping of transport and other experiments with Raman spectroscopy will be highly desirable to further our understanding of the electronic and vibrational structure of graphene oxide.

## REFERENCES

- [1]. Novoselov, K. S.; Geim, A. K.; Morozov, S. V.; Jiang, D.; Zhang, Y.; Dubonos, S. V.; Grigorieva, I. V.; Firsov, A. A. *Science* **2004**, 306, 666–669.
- [2]. Geim, A. K.; Novoselov, K. S. *Nat. Mater.* **2007**, 6, 183–191.
- [3]. Stankovich, S.; Dikin, D. A.; Dommett, G. H. B.; Kohlhaas, K. M.; Zimney, E. J.; Stach, E. A.; Piner, R. D.; Nguyen, S. T.; Ruoff, R. S. *Nature* **2006**, 442, 282–286.
- [4]. Lee, C.; Wei, X.; Kysar, J. W.; Hone, J. *Science* **2008**, 321, 385–388.
- [5]. Berger, C.; Song, Z.; Li, X.; Wu, X.; Brown, N.; Naud, C.; Mayou, D.; Li, T.; Hass, J.; Marchenkov, A. N.; Conrad, E. H.; First, P. N.; de Heer, W. A. *Science* **2006**, 312, 1191–1196.
- [6]. Reina, A.; Jia, X.; Ho, J.; Nezich, D.; Son, H.; Bulovic, V.; Dresselhaus, M. S.; Kong, J. *Nano Lett.* **2009**, 9, 30–35.
- [7]. Li, X.; Cai, W.; An, J.; Kim, S.; Nah, J.; Yang, D.; Piner, R.; Velamakanni, A.; Jung, I.; Tutuc, E.; Banerjee, S. K.; Colombo, L.; Ruoff, R. S. *Science* **2009**, 324, 1312–1314.
- [8]. Son, Y.-W.; Cohen, M. L.; Louie, S. G. *Phys. Rev. Lett.* **2006**, 97, 216803–4.
- [9]. Nakada, K.; Fujita, M.; Dresselhaus, G.; Dresselhaus, M. S. *Phys. Rev. B* **1996**, 54, 17954–17961.
- [10]. Yang, L.; Park, C.-H.; Son, Y.-W.; Cohen, M. L.; Louie, S. G. *Phys. Rev. Lett.* **2007**, 99, 86801–4.
- [11]. Li, X.; Wang, X.; Zhang, L.; Lee, S.; Dai, H. *Science* **2008**, 319, 1229–1232.

- [12]. Jiao, L.; Zhang, L.; Wang, X.; Diankov, G.; Dai, H. *Nature* **2009**, 458, 877–880.
- [13]. Wang, X.; Li, X.; Zhang, L.; Yoon, Y.; Weber, P. K.; Wang, H.; Guo, J.; Dai, H. *Science* **2009**, 324, 768–771.
- [14]. Wilder, J. W. G.; Venema, L. C.; Rinzler, A. G.; Smalley, R. E.; Dekker, C. *Nature* **1998**, 391, 59–62.
- [15]. Odom, T. W.; Huang, J.-L.; Kim, P.; Lieber, C. M. *Nature* **1998**, 391, 62–64.
- [16]. Terrones, M. *Nature* 2009, 458, 845–846.
- [17]. Han, M. Y.; Ozyilmaz, B.; Zhang, Y.; Kim, P. *Phys. Rev. Lett.* **2007**, 98, 206805–4.
- [18]. Kosynkin, D. V.; Higginbotham, A. L.; Sinitskii, A.; Lomeda, J. R.; Dimiev, A.; Price, B. K.; Tour, J. M. *Nature* **2009**, 458, 872–876.
- [19]. Bai, J.; Duan, X.; Huang, Y. *Nano Lett.* **2009**, 9, 2083–2087.
- [20]. Cano-Marquez, A. G.; Rodríguez-Macas, F. J.; Campos-Delgado, M. J.; Spinoza-Azules, C. G.; Tristán-López, F.; Ramírez-González, D.; Cullen, D. A.; Smith, D. J.; Terrones, M.; Vega-Cantu, Y. I. *Nano Lett.* **2009**, 9, 1527–1533.
- [21]. K. Andre Mkhoyan, Alexander W. Contryman, John Silcox, Derek A. Stewart, Goki Eda, Cecilia Mattevi, Steve Miller, and Manish Chhowalla *Nano Lett.*, **2009**, 9 (3), 1058-1063 • DOI: 10.1021/nl8034256
- [22]. M. Cardona, "Resonance phenomena", in *Light Scattering in Solids 11*, edited by M. Cardona and G. Giintherodt (Springer, Berlin, **1982**), vol. 50 of *Topics in Applied Physics*, p. 19.
- [23]. A. Pinczuk and E. Burstein, "Fundamentals of inelastic light scattering in semiconductors and insulators", in *Light Scattering in Solids I* (Springer Verlag, Berlin, **1983**), vol. 8 of *Topics in Applied Physics*, p. 23, 2 edn.
- [24]. R. M. Martin and L. M. Falicov, "Resonant Raman scattering", in *Light Scattering in Solids I: Introductory Concepts*, edited by M. Cardona (Springer-Verlag, Berlin Heidelberg New York, **1983**), vol. 8 of *Topics in Applied Physics*, p. 79, 2 edn.
- [25]. M. Damnjanovic, I. Bozovic, and N. Bozovic, "Selection rules for polymers and quasi one-dimensional crystals: II. Kronecker product for the line groups isogonal to  $D_n$ ", *J. Phys. A: Math. Gen.* **17**, 747 (**1984**).
- [26]. J. Maullzsch, S. Reich, and C. Thomsen, "Chirality selective Raman scattering of the D-mode in carbon nanotubes", *Phys. Rev. B* **64**, 12 1407(R) (**2001**).
- [27]. Y.-N. Chiu, "General orientation dependence of Rayleigh and Raman scattering by linear molecules in arbitrary electronic states", *J. Opt. Soc. Am.* **60**, 607 (**1970**).
- [28]. C. Kane-Maguire and J. A. Koningstein, "On the vibroelectric Raman effect", *J. Chem. Phys.* **59**, 1899 (**1973**).
- [29]. S. Reich, C. Thomsen, G. S. Duesberg, and S. Roth, "Intensities of the Raman active modes in single and multiwall nanotubes", *Phys. Rev. B* **63**, R041401 (**2001**).
- [30]. S. Reich and C. Thomsen, "Tensor invariants in resonant Raman scattering on carbon nanotubes", in *Proc. 25th ICPS, Osaka*, edited by N. Miura and T. Ando (Springer, Berlin, **2001**), p. 1649
- [31]. V. Heine, *Group Theory in Quantum Mechanics: An Introduction to its Present Usage* (Pergamon, Oxford, **1977**).
- [32]. D. M. Brink and G. R. Satchler, *Angular Momentum* (Oxford, New York, **1993**), 3 edn.
- [33]. J. Nestor and T. G. Spiro, "Circularly polarized Raman spectroscopy: Direct determination of antisymmetric scattering in the resonance Raman spectrum of ferrocyclochrom c", *J. Raman Spectroscopy* **1**, 539 (**1973**).
- [34]. Cristina Gomez-Navarro, R. Thomas Weitz, Alexander M. Bittner, Matteo Scolari, Alf Mews, Marko Burghard, and Klaus Kern, "Electronic Transport Properties of Individual Chemically Reduced Graphene Oxide Sheets" *Nano Lett.* **2007** Vol. 7, No. 11 3499-3503
- [35]. Tuinstra, R.; Koenig, J. L. *J. Chem. Phys.* **1970**, **53**, 1126.

[36]. Szabo, T.; Berkesi, O.; Forgo, P.; Josepovits, K.; Sanakis, Y.; Petridis, D.; Dekany, I. *Chem. Mater.* **2006**, 18, 2740.